Genotype-Dependent Variability in Residual Cone Structure in Achromatopsia: Toward Developing Metrics for Assessing Cone Health

Adam M. Dubis,[1,2] Robert F. Cooper,[3] Jonathan Aboshiha,[1,2] Christopher S. Langlo,[4] Venki Sundaram,[1,2] Benjamin Liu,[5] Frederick Collison,[6] Gerald A. Fishman,[6] Anthony T. Moore,[1,2] Andrew R. Webster,[1,2] Alfredo Dubra,[3,5,7] Joseph Carroll,[3,4,5,7] and Michel Michaelides[1,2]

[1]Moorfields Eye Hospital, London, United Kingdom
[2]UCL Institute of Ophthalmology, University College London, London, United Kingdom
[3]Department of Biomedical Engineering, Marquette University, Milwaukee, Wisconsin, United States
[4]Department of Cell Biology, Neurobiology and Anatomy, Medical College of Wisconsin, Milwaukee, Wisconsin, United States
[5]Department of Ophthalmology, Medical College of Wisconsin, Milwaukee, Wisconsin, United States
[6]The Pangere Center for Hereditary Retinal Diseases, The Chicago Lighthouse for People Who Are Blind or Visually Impaired, Chicago, Illinois, United States
[7]Department of Biophysics, Medical College of Wisconsin, Milwaukee, Wisconsin, United States

Correspondence: Adam M. Dubis, UCL Institute of Ophthalmology, 11-43 Bath Street, London, EC1V 9EL, UK; a.dubis@ucl.ac.uk.

Submitted: February 22, 2014
Accepted: September 21, 2014

Citation: Dubis AM, Cooper RF, Aboshiha J, et al. Genotype-dependent variability in residual cone structure in achromatopsia: toward developing metrics for assessing cone health. *Invest Ophthalmol Vis Sci*. 2014;55:7303–7311. DOI:10.1167/iovs.14-14225

Purpose. Gene therapy trials for inherited photoreceptor disorders are planned. Anatomical metrics to select the best candidates and outcomes are needed. Adaptive optics (AO) imaging enables visualization of photoreceptor structure, although analytical tools are lacking. Here we present criteria to assess residual photoreceptor integrity in achromatopsia (ACHM).

Methods. Two AOSLOs, at the Medical College of Wisconsin and Moorfields Eye Hospital, were used to image the photoreceptor mosaic of 11 subjects with ACHM and 7 age-matched controls. Images were obtained, processed, and montaged using previously described methods. Cone density and reflectivity were quantified to assess residual cone photoreceptor structure.

Results. All subjects with ACHM had reduced numbers of cone photoreceptors, albeit to a variable degree. In addition, the relative cone reflectivity varied greatly. Interestingly, subjects with *GNAT2*-associated ACHM had the greatest number of residual cones and the reflectivity of those cones was significantly greater than that of the cones in the subjects with *CNGA3/CNGB3*-associated ACHM.

Conclusions. We present cone reflectivity as a metric that can be used to characterize cone structure in ACHM. This method may be applicable to subjects with other cone disorders. In ACHM, we hypothesize that cone numerosity (and/or density) combined with cone reflectivity could be used to gauge the therapeutic potential. As gene replacement would not be expected to add cones, reflectivity could be a more powerful AO-metric for monitoring the cellular response to treatment and could provide a more immediate indicator of efficacy than behavioral measures, which may take longer to change.

Keywords: cones, image analysis, genetic diseases

Achromatopsia (ACHM) is an autosomal recessive condition that affects approximately 1 in 30,000 people.[1] Achromatopsia presents at birth or early infancy and is characterized by pendular nystagmus, poor visual acuity, marked photophobia, and absent/markedly reduced color vision. Fundus examination is usually normal, and electrophysiological testing demonstrates absent cone responses and normal rod function.[2] To date, five genes encoding components of the cone-specific phototransduction cascade have been associated with ACHM. The two most common causative genes are *CNGA3*[3] and *CNGB3*,[4] which encode the α- and β-subunits of the cGMP-gated cation channel, respectively. Disease-causing variants also have been identified in *GNAT2*, which encodes the α-subunit of transducin,[5] *PDE6C*, encoding the α-subunit of cGMP phosphodiesterase (PDE),[6] and *PDE6H*, which encodes the γ-subunit of cGMP PDE.[7] Sequence variants in *CNGA3* and *CNGB3* account for approximately 70% to 80% of ACHM,[8] *GNAT2* accounting for approximately 1%,[5] and *PDE6C*, *PDE6H*, or unknown causes accounting for the remaining cases.

The relatively limited histopathologic investigations of photoreceptor morphology in ACHM describe a wide range of observations. Galezowski[9] reported a complete absence of cones, whereas Larsen[10] identified malformed foveal cones and normal peripheral cones. Harrison et al.[11] found misshaped and reduced numbers of cones throughout the retina. In contrast, Falls et al.[12] described normal numbers of misshaped foveal

cones and a normal number of peripheral cones. Most recently, Glickstein and Heath[13] reported no evidence of foveal cones and reduced numbers of peripheral cones. Importantly, these reports predate knowledge of the underlying molecular genetic basis of ACHM.[9–13]

Adaptive optics (AO) imaging enables direct visualization of the rod and cone photoreceptors in the living human eye.[14,15] This technology has been used to reexamine photoreceptor morphology in ACHM. This was first undertaken in a single subject with *CNGB3*-associated ACHM by Carroll et al.,[16] who observed a severely disrupted cone mosaic in the fovea and parafovea. Merino et al.[17] also assessed a single *CNGB3* subject, and noted dark spaces in the mosaic that were spaced too far apart to be "normal" cones, and the visible cells were too closely spaced to be cones and were posited to be rods. A study of nine molecularly confirmed (*CNGA3* and *CNGB3*) subjects by Genead et al.[18] reported residual cone structure in all but one of the subjects imaged, although most of the cones had reduced reflectance. More recently, Scoles et al.[19] used a novel "split detector" AO scanning light ophthalmoscopy (AOSLO) technique to visualize residual inner segment structure within the dark spaces seen on confocal images. These imaging results support the idea that cone structure in ACHM is disrupted, but not absent. Although the degree of residual cone structure is variable, no genotype-dependent differences have been reported. Although methods of quantifying cones that are normal in appearance are well established, techniques for quantifying the residual abnormal cone structure in ACHM are lacking.[20–23] Such tools are needed, in light of recent studies demonstrating effectiveness of gene replacement therapy in restoring cone function in multiple animal models of ACHM and planned initiation of human trials in the near future.[24–27]

Here we used AO imaging to assess photoreceptor integrity in subjects with genetically confirmed ACHM, including subjects with ACHM associated with *GNAT2* variants. We show evidence suggesting a genotype-phenotype correlation with respect to the degree of residual photoreceptor structure. As proposed by Genead et al.,[18] we evaluated the intensity of parafoveal photoreceptors as an indicator of cone health. Here we show that this quantification can differentiate between different ACHM genotypes. Such metrics may play a role in monitoring retinal morphology after therapeutic interventions, including gene replacement therapy, and may be helpful in characterizing cone structure in other retinal diseases

Methods

Subject Demographic Data

Eleven subjects with molecularly proven ACHM were included in this study, recruited from Moorfields Eye Hospital, United Kingdom; The Pangere Center for Hereditary Retinal Diseases at The Chicago Lighthouse, USA; and the Medical College of Wisconsin, USA. Seven additional subjects with normal vision were recruited to serve as controls. The study adhered to the Tenets of the Declaration of Helsinki; was approved by the local ethics committees of Moorfields Eye Hospital, Medical College of Wisconsin, and Western Institutional Review Board; and was performed with the informed consent of all subjects. Subject demographic data are given in Table 1. To genetically confirm the clinical diagnosis, conventional direct Sanger sequencing of exons and exon-intron boundaries of *CNGA3*, *CNGB3*, *GNAT2*, and *PDE6C* was undertaken using previously published methods.[5,28] Electrophysiological testing was previously performed on all subjects to confirm the complete achromatopsia diagnosis in these subjects.

Table 1. Summary of Demographic Data

Subject No.	Age, y	Sex	Axial Length, mm	Gene	Allele 1/ Allele 2	Foveal Hypoplasia	ELM Ratio		ISe Ratio	
							1 mm	1.5 mm	1 mm	1.5 mm
JC_0825	26	M	24.2	n/a	Normal	N	ND	ND	ND	ND
MM_0059	43	F	23.99	n/a	Normal	N	ND	ND	ND	ND
MM_0093	22	M	25.94	n/a	Normal	N	ND	ND	ND	ND
MM_0102	25	F	25.86	n/a	Normal	N	ND	ND	ND	ND
JC_0822	66	M	24.50	n/a	Normal	N	ND	ND	ND	ND
JC_0823	52	F	22.32	n/a	Normal	N	ND	ND	ND	ND
JC_0864	56	M	24.01	n/a	Normal	N	ND	ND	ND	ND
JC_1064	52	M	24.61	*GNAT2*	c.843-844insAGTC-p.His282Ser fs*11 / c.843-844insAGTC-p.His282Ser fs*11	N	0.58	0.64	1.99	2.57
JC_1065	43	M	23.55	*GNAT2*	c.843-844insAGTC-p.His282Ser fs*11 / c.843-844insAGTC-p.His282Ser fs*11	N	0.74	0.5	2.68	3.15
JC_1240	24	F	21.62	*CNGA3*	c.1351dupG fs*1 / c1279C>T-p.Arg427Cys	N	ND	ND	ND	ND
MM_0002	34	F	24.38	*CNGA3*	c.1443-1444insC-p.Ile482His fs*6 / c.1706G>A-p.Arg569His	Y	0.55	0.56	1.02	1.21
MM_0009	9	F	21.43	*CNGA3*	c.536T>A-p.Val179Asp / c.536T>A-p.Val179A	N	0.79	1.12	1.19	1.53
MM_0015	25	F	25.11	*CNGA3*	c.848G>A-p.Arg283Gln / c.667C>T-p.Arg223Cys	Y	0.66	0.64	1.66	1.73
JC_1208	16	M	23.52	*CNGB3*	c.1148delC-Thr383 fs*1 / c.1148delC-Thr383 fs*1	Y	ND	ND	ND	ND
MM_0004	23	M	23.67	*CNGB3*	c.1148delC-p.Thr383Ile fs*13 / c.1148delC-p.Thr383Ile fs*13	Y	0.62	0.54	1.55	1.59
MM_0005	24	M	22.65	*CNGB3*	c.1148delC-p.Thr383Ile fs*13 / c.607-608insT-p.Arg203Leu fs*3	N	0.54	0.57	0.80	0.67
MM_0029	14	F	21.8	*CNGB3*	c.595delG-p.Glu199Ser fs*3 / c.1148delC-p.Thr383Ile fs*13	Y	0.57	0.56	1.28	1.73
MM_0085	17	F	23.7	*CNGB3*	c.1148delC-p.Thr383Ile fs*13 / c.1006G>T- p.Glu336 Ter	Y	0.93	0.83	2.07	1.75

The cDNA is numbered according to Ensembl transcript ID: *CNGA3* ENST00000409937; *CNGB3* ENST00000320005; *GNAT2* ENST00000351050.
F, female; M, male; N, no; n/a, not applicable; ND, not determined; Y, yes.

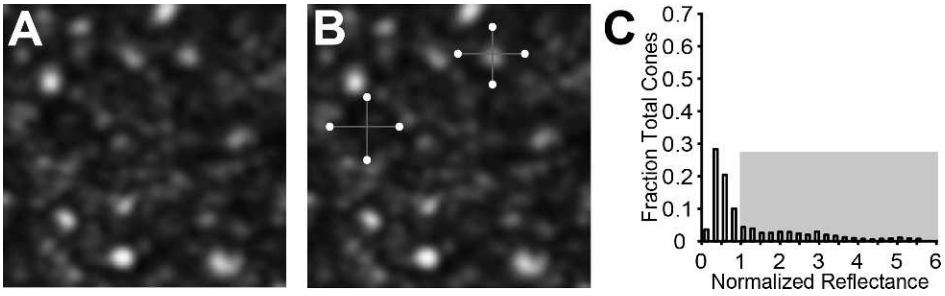

FIGURE 1. Measuring cone photoreceptor reflectance in ACHM. Cone photoreceptors were manually identified from AOSLO images (**A**). The displayed image is from a subject with *GNAT2*-associated ACHM (JC_1064). The diameter of each cone was measured along two axes (**B**). The percentage of cells with a reflectance greater than 1 (*gray-shaded region*) was calculated (**C**).

Spectral Domain Optical Coherence Tomography Imaging

All subjects had macular spectral domain optical coherence tomography (SDOCT) scans using an Envisu SDOCT system (Bioptigen, Inc., Morrisville, NC, USA). Line scan sets were acquired (1000 A-scans/B-scan; 100 repeated B-scans) through the foveal center, and this location was confirmed based on inspection of an accompanying high-density volume-scan. Scans were registered and averaged as previously described to reduce speckle noise in the image.[29] The lateral scale of each image was estimated using the axial length information obtained from the Zeiss IOL Master (Carl Zeiss Meditec, Dublin, CA, USA). Foveal hypoplasia was graded based on previously published reports; in short, subjects were considered to have foveal hypoplasia if more than a single inner retinal layer was present at the foveal center.[30] Subjects JC_1064 (subject 37), JC_1065 (subject 35), MM_0002 (subject 16), MM_0004 (subject 28), MM_0005 (subject 29), MM_0009 (subject 4), MM_0015 (subject 8), MM_0029 (subject 21), and MM_0085 (subject 22) were previously included in an SDOCT study in which the intensity of the inner segment ellipsoid band (ISe) and external limiting membrane (ELM) were measured from Heidelberg Spectralis images (Heidelberg Engineering, Heidelberg, Germany) as previously described.[30,31]

Adaptive Optics Imaging

Two AOSLOs were used for imaging. One was a previously described instrument at the Medical College of Wisconsin.[32,33] The other instrument was a newly constructed, identical system at Moorfields Eye Hospital. All subjects were dilated and accommodation suspended using one drop each of phenylephrine hydrochloride (2.5%) and tropicamide (1%). The imaging source was a 790-nm super luminescent diode (Superlum Ireland, Carrigtwohill, County Cork, Ireland). Image sequences were processed to remove distortions induced by the sinusoidal motion of the resonant scanner by estimating the distortion from images of a calibrated Ronchi ruling and then resampling the images over a grid of equally spaced pixels. These image sequences were registered to improve signal-to-noise as previously described.[34] The registered images from each image sequence were then combined into a single montage (Adobe Photoshop; Adobe Systems, Inc., San Jose, CA, USA). No brightness or contrast changes were applied to images. Montages

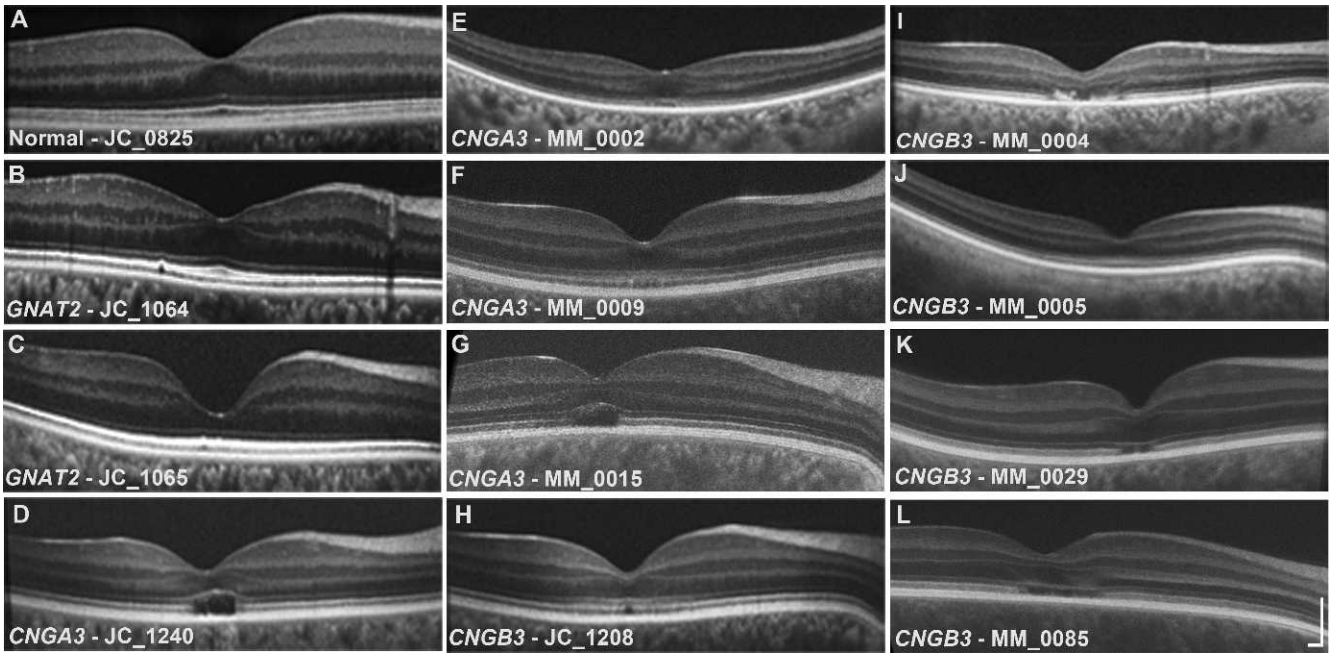

FIGURE 2. Macular SDOCT images for a healthy subject and all subjects with ACHM. Images were graded for the presence or absence of foveal hypoplasia (presence of more than a single inner retinal layer extending through the foveal region). Several subjects (Table 1) were previously evaluated for ISe and ELM band reflectivity. *Scale bar*: 200 μm.

Investigative Ophthalmology & Visual Science

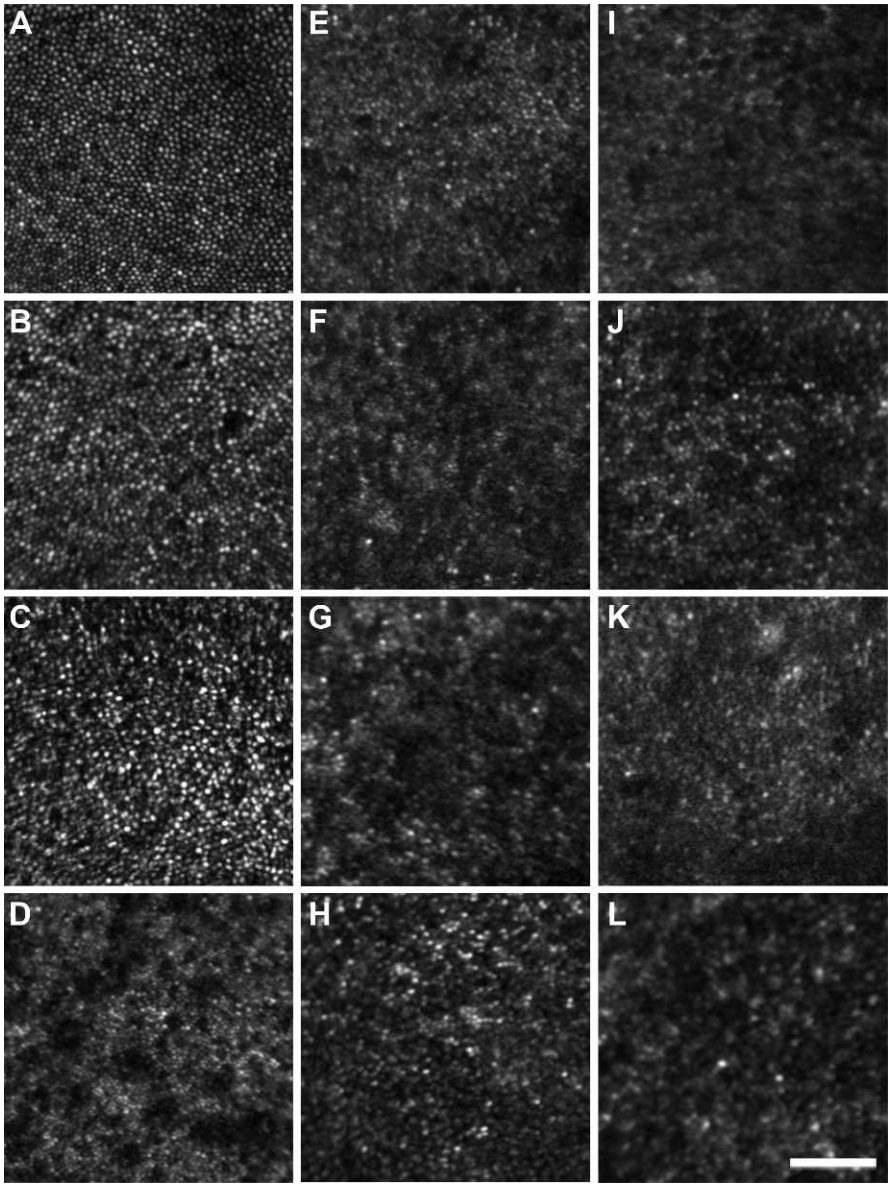

Figure 3. Sample AOSLO images 0.65° from fixation. (**A**) Healthy control. (**B**, **C**) Subjects with *GNAT2* mutations (JC_1064 and JC_1065, respectively). (**D**–**G**) Achromats with *CNGA3* mutations (JC_1240, MM_0002, MM_0009, and MM_0015). (**H**–**L**) Achromats with *CNGB3* mutations (JC_1208, MM_0004, MM_0005, MM_0029, and MM_0085). *Scale bar*: 50 μm.

of images consisted of a minimum approximately 4° box at fixation and strings of images extending 10° temporally and 5° superiorly. The relative locus of fixation was defined as the center of the image acquired when the subject was instructed to look at the center of the imaging raster. Although many subjects with ACHM have considerable nystagmus, the subjects used in this study had minimal nystagmus, allowing visualization of locus of fixation.

Analysis of Photoreceptor Reflectance

In AOSLO images of the photoreceptor mosaic, normal rods and foveal cones appear as small round structures with a roughly Gaussian reflectivity profile.[14,35] Away from the fovea, cones generally appear as a bright reflective structure of variable shape and size, surrounded by a dark ring[35] (Supplementary Figs. S1, S2). The extent of the dark ring has been shown to correspond to the cone inner segment,[19] whereas the brighter central reflective core is thought to originate from reflections within or near the photoreceptor outer segment.[36] Cone reflectance was assessed using images acquired approximately 4° to 6° temporal to fixation, as outlined in Figure 1. For each subject, the boundaries of between 750 and 1140 (average 955) cones were manually selected along two orthogonal axes of the cell using ImageJ (http://imagej.nih.gov/ij/; provided in the public domain by the National Institutes of Health, Bethesda, MD, USA) (Fig. 1B).[37] The "center" of the cone was identified as the intersection of the two axes. The reflectance of each cone was defined as the mean reflectance of all pixels within a circle centered on the cone, whose diameter was 90% of that cell's diameter (as defined by the user-selected points). The use of the 90% diameter allowed inclusion of the signal from as much of the cone as possible without being influenced by the rods, which surround the cones in the peripheral retina.

To assess rod reflectivity, rods were manually identified in the mosaic using ImageJ (National Institutes of Health)[37]

Investigative Ophthalmology & Visual Science

Table 2. Subject Photoreceptor Reflectance Data

	Cone Density, Cones/mm²		Cone Reflectance				
Subject No.	0.65°	5°	Average	SD	% > 1	Cones Sampled	Rods Sampled
JC_0825	76,694	13,884	2.49	0.73	99.8	1,008	1,011
MM_0059	78,678	12,810	2.46	0.83	98.8	1,025	1,027
MM_0093	88,595	14,165	2.92	0.90	98.0	1,015	1,021
MM_0102	73,058	13,496	2.06	0.57	98.6	1,021	1,015
JC_0822	87,934	16,860	2.07	0.60	92.4	1,003	1,012
JC_0823	73,388	15,868	2.56	0.86	98.3	1,011	1,050
JC_0864	82,645	17,190	2.23	0.62	97.4	1,005	1,049
JC_1064	65,785	10,273	0.95	0.87	28.8	784	1,002
JC_1065	59,504	11,612	1.90	1.89	46.7	848	1,002
JC_1240	12,231	5,959	0.59	0.32	1.2	995	986
MM_0002	10,579	5,620	0.56	0.31	1.1	760	1,018
MM_0009	19,504	6,281	0.35	0.13	0.1	1,111	1,020
MM_0015	17,190	4,959	0.40	0.16	0.9	1,140	1,017
JC_1208	11,570	6,959	0.34	0.11	0.0	869	990
MM_0004	13,554	4,250	0.35	0.15	0.8	750	1,010
MM_0005	12,893	4,989	0.36	0.12	0.1	820	999
MM_0029	18,843	7,603	0.47	0.14	0.8	1,013	1,016
MM_0085	18,512	7,273	0.48	0.17	0.9	1,012	1,019

Table rows separated by genotype (normal, *GNAT2*, *CNGA3*, *CNGB3*). % >1 is the percentage of reflectance profiles with a normalized reflectance greater than 1; Cone(s) indicate cone photoreceptor(s) and Rod(s) indicate rod photoreceptor(s).

(Supplementary Fig. S1). The center location of each rod was identified as the local maximum within a distance of three pixels from the user-selected rod center. The reflectance of each rod was defined as the mean reflectance of all pixels within a circle centered on the rod, whose diameter was 3.3 μm. This diameter was selected as it represents the approximate diameter of a rod photoreceptor at the assessed locations.[33] On average, 1015 (range, 986–1050) rod photoreceptors were identified in each subject.

The reflectivity values for rod and cone photoreceptors were normalized to the average noncone intensity of the image. To do this, the area void of vessels was selected, then the cone areas were masked, and the remainder of the image intensity was averaged. Thus, cells with a normalized reflectivity less than 1 were dimmer than the image average, whereas cells with a normalized reflectivity greater than 1 were brighter than the image average. An example is shown in Figure 1C. To quantify the photoreceptor reflectivity, we calculated the average cone and rod reflectivity and determined the percentage of the total population with a reflectance greater than 1.

Cone Density

Cone density was measured manually at 0.65° and 5° from fixation. For counting purposes in this study, an object was considered a "cone" regardless of the apparent intensity of the central reflective core. To remove the effect of edge artifacts in our cone counts, cone photoreceptors were identified over an 80 × 80-μm region, and then analyzed over a 55 × 55-μm area.

Statistical Analysis

Statistical analysis was done using JMP, version 11 (SAS Institute, Inc., Cary, NC, USA). The Kolmogorov-Smirnov test was used to test each subject's reflectance for normality. To evaluate statistical significance in photoreceptor reflectivity between subjects of the same genotype, a one-way ANOVA test was done for the subjects with *CNGB3* and *CNGA3* mutations. Because only two subjects with *GNAT2* were included, a Mann-Whitney *U* was performed. Comparison of photoreceptor reflectivity across genotypes was performed using a Kruskal-Wallis one-way ANOVA with Bonferroni correction for multiple comparisons.

Results

Disease-causing variants were identified in *CNGA3* in four subjects, in *CNGB3* in five subjects, and in *GNAT2* in two brothers (Table 1). Foveal integrity was variable; both subjects with *GNAT2* mutations and two subjects with *CNGA3* mutations had normal foveal excavation, whereas the other subjects had some degree of foveal hypoplasia. Both subjects with *GNAT2* mutations and one of the subjects with *CNGB3* mutations (MM_0005) had continuous ISe and ELM retinal bands throughout the macula, whereas all other subjects exhibited some degree of disruption at the foveal center. Macular SDOCT scans from one healthy and all subjects with ACHM are shown in Figure 2, and previously reported relative ISe and ELM band intensities for selected subjects are given in Table 1.

Qualitative and Quantitative Mosaic Assessment With AO Imaging

All ACHM subjects had photoreceptor mosaic disruption at the presumed center of their photoreceptor mosaic, albeit to a variable degree. Photoreceptor images acquired 0.65° from fixation are shown in Figure 3. All subjects with ACHM had a reduced number of photoreceptors compared with the healthy controls. The images of the subjects with *GNAT2* mutations (Figs. 3B, 3C) were particularly noteworthy, with photoreceptor density being only slightly lower than normal (Table 2) and a near contiguous mosaic was present at the fovea. This remarkable finding was in direct contrast to the other ACHM genotypes, all of whom had markedly reduced cone structure at the parafoveal location. Cone density for our healthy subjects ranged from 73,058 to 88,595 cones/mm² compared with 59,504 to 65,785 cones/mm² for the subjects with *GNAT2* mutations. In direct contrast, central cone density was greatly

Investigative Ophthalmology & Visual Science

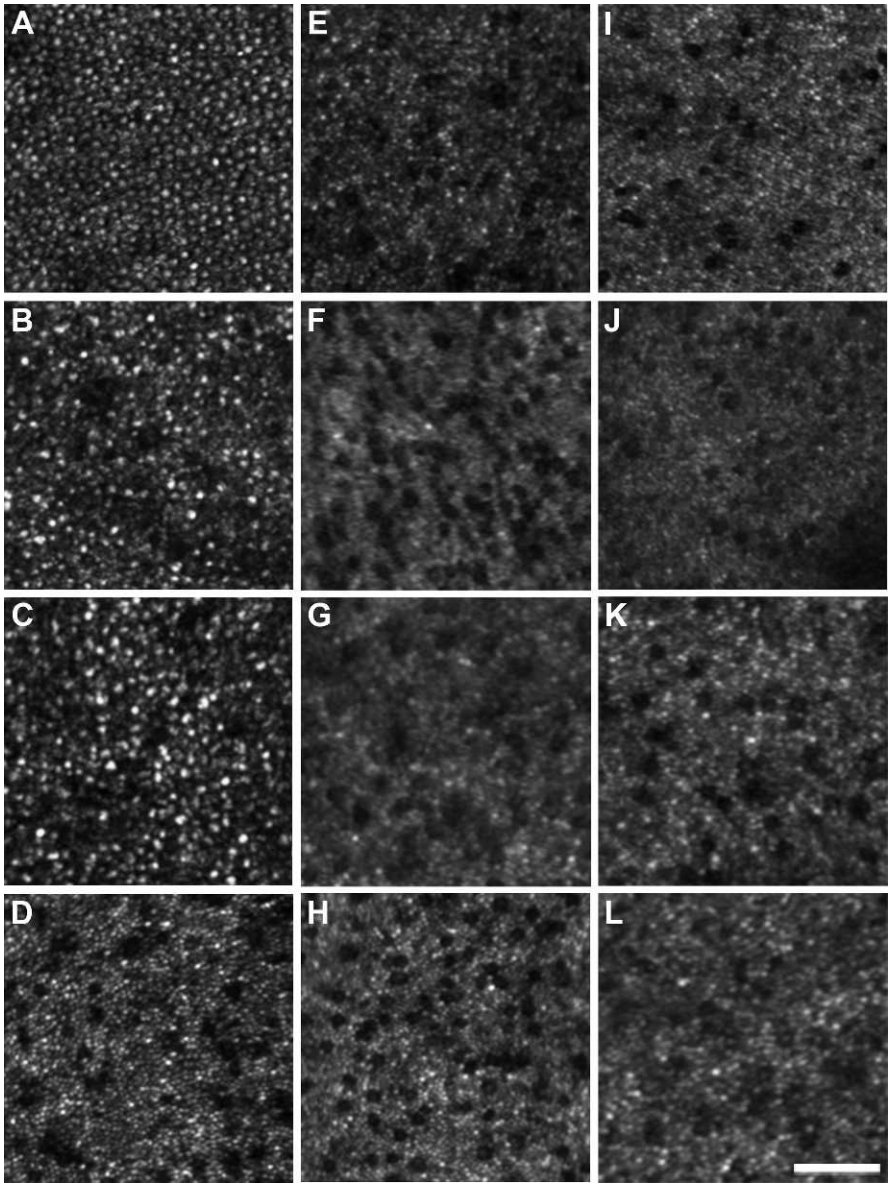

FIGURE 4. Sample AOSLO images 5° from fixation. (**A**) Healthy control. (**B**, **C**) Achromats with *GNAT2* mutations (JC_1064 and JC_1065, respectively). (**D**–**H**) Achromats with *CNGA3* mutations (JC_1240, MM_0002, MM_0009, and MM_0015). (**H**–**L**) Achromats with *CNGB3* mutations (JC_1208, MM_0004, MM_0005, MM_0029, and MM_0085). *Scale bar*: 50 μm.

reduced in the other ACHM subjects (10,579–19,504 cones/mm^2). Specific subject values are present in Table 2. A similar trend was seen in images 5° from fixation, as shown in Figure 4. The healthy subjects had cone density that ranged from 12,810 to 17,190 cones/mm^2, whereas the two subjects with *GNAT2* mutations had densities of 10,273 and 11,612 cones/mm^2. In contrast, the subjects with *CNGA3* and *CNGB3* mutations had density values ranging between 4250 and 7603 cones/mm^2. In addition, the qualitative appearance of the residual parafoveal cone structure varied significantly among *CNGA3*, *CNGB3*, and *GNAT2* groups (Fig. 4).

Photoreceptor Reflectivity

The average cone photoreceptor reflectance, SD, and percentage of cells with an average reflectance greater than 1 are shown in Table 2. The retinal areas analyzed are shown in Figure 4, with the individual cone cells that we measured being further illustrated in Supplementary Figure S2. Average reflectance (±SD) for the healthy subjects was 2.40 (±0.31). On average, in the healthy subjects, 97.6% of the cones had a normalized reflectance that was greater than 1. There was no statistical difference in cone reflectance among healthy subjects ($P > 0.05$). In keeping with previous qualitative observations of cone reflectivity in ACHM, the cones in subjects with *CNGA3/B3* mutations had abnormal reflectance profiles, with less than 1.5% of their cones having reflectance values greater than 1 (Table 2). There was no difference in average cone reflectance between subjects within either the *CNGA3* ($P > 0.05$, one-way ANOVA) or *CNGB3* ($P > 0.05$, one-way ANOVA) group. There was also no difference detected between the *CNGA3* and *CNGB3* ($P = 0.062$, Mann-Whitney *U*) groups. In contrast, between 28% and 47% of the cones in the subjects with *GNAT2* mutations had a reflectance greater than 1 (Table 2). Average cone reflectance was greatest for the healthy subjects; with subjects with *GNAT2*-associated ACHM

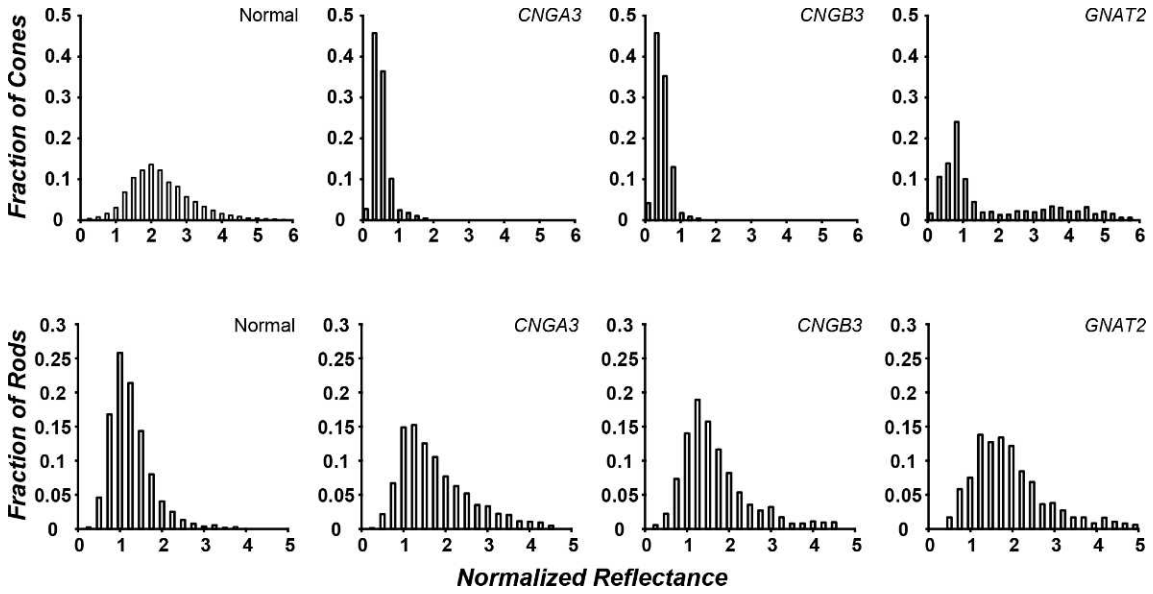

FIGURE 5. Genotype-dependent differences in cone photoreceptor reflectance in ACHM. Photoreceptor reflectance was binned and the number of cells was plotted as a fraction of the total number of cells. Data were averaged across subjects by genotype. (*Top*) Cone reflectivity was variable between genotypes. Subjects with *CNGA3/B3* mutations showed, on average, lower reflectance than normal. Subjects with *GNAT2* mutations also showed reduced reflectance on average compared with healthy subjects, but greater reflectance and variability than *CNGA3/B3*. (*Bottom*) Rod reflectivity was not different from the healthy control in all ACHM genotypes.

falling between healthy and the *CNGA3/B3* subjects (Fig. 5). The distribution of normalized reflectance values for all achromats was statistically different from the healthy subjects (*GNAT2* $P = 0.0013$; *CNGB3* $P < 0.0001$; *CNGA3* $P < 0.0001$, Mann-Whitney *U*). This difference in cone reflectivity is consistent with previously reported differences in the relative intensity of the ISe band on SDOCT images.[30] There was no difference in average rod reflectance between subjects within or between groups ($P > 0.05$, one-way ANOVA); however, this is to be expected given our normalization methods.

Discussion

In this study, we present the first evidence of a genotype-dependent difference in residual cone structure in ACHM. Whether our findings extend to other subjects with *GNAT2*-associated ACHM or are restricted to the specific mutation reported here remains to be seen. It is important to note that there were large differences between the two subjects with *GNAT2* mutations, who were brothers; nevertheless, they were both significantly different from the other genotypes examined. However, in keeping with our findings of improved cone structure (greater cone density, higher average cone reflectance, and increased reflectance of the ISe band on SDOCT), in-depth psychophysical assessment has suggested *GNAT2*-associated ACHM has slightly greater residual cone function than *CNGA3/B3*-associated ACHM,[38] which suggests that our structural findings might be expected to extend to other subjects with *GNAT2* mutations. Moreover, our findings demonstrate the importance of assessing photoreceptor structure on an *individualized* basis. We also present data supporting the use of cell reflectivity as a metric to characterize the residual cone integrity in subjects with ACHM.[18]

In developing metrics to quantify photoreceptor reflectance, the method for measuring the reflectance of a cell and the normalization process are important factors. Ideally, a nonphotoreceptor layer would be imaged simultaneously with the photoreceptor layers using the exact same light source and detectors, and subsequently used for normalization. This normalization also would include residual AO correction error, detector sensitivity, and tear film integrity. It also would thereby allow for independent measurements of rod and cone cell reflectivity. Unfortunately, current imaging capabilities do not allow these methods to be implemented. Therefore, the methods used are associated with some inherent limitations with respect to normalized reflectance measurements. For measuring the reflectance of peripheral cones, we chose to average reflectance over as much of the cone diameter as possible. In a treatment that might be expected to improve cone structure or function, we would predict that the cone reflectivity would change. Given the heterogeneous nature of cone reflectance profiles, we felt a larger sampling area would provide the best foundation for making future follow-up measures. Another approach could have been actually analyzing the reflective core, perhaps fitting to a Difference of Gaussian profile. Although this would remove some of the subjectivity in defining the cone diameter, it has the disadvantage that differences in the shape of the profile would be confounded with differences in intensity. In the future, it may be possible to use the inner segment diameter measured using split detector AOSLO to determine the measurement area on a cone-by-cone basis.[19] Regardless of the method used, it is important that the parameters be openly disclosed to allow comparison across research groups but also to ensure consistency in measurement techniques in a population over time. Normalization is equally important, and we opted to mask the cones. The rationale is that in ACHM, the expectation is that the cones would change reflectivity in response to treatment, thus including them in the normalization would confound the measurement. It may be that to apply a similar technique to rod disorders, normalizing to a signal in the inner retina might be an even better choice, as has been done in similar OCT studies.[30,39] Additional reports from a number of other conditions also have reported disrupted cone reflectivity,[18,35,40–42] so the methods developed here also may be

applicable to these disorders; however, extensive repeatability and reproducibility studies in each disorder must be done to ensure the robustness of photoreceptor reflectivity analysis before their potential application to clinical trials in each pathology. It may be possible that this method would be useful only for ACHM; further studies must be done.

Although our study is limited by small sample size, we have demonstrated clear differences in the cone mosaic between the *CNGA3/B3* and *GNAT2* subjects. Another limitation of this study is that it is cross-sectional. Several studies have questioned whether ACHM is a stationary or progressive disease.[1,43] Two large cross-sectional OCT studies have been undertaken[44,45] that suggest inexorable disease progression by assessing outer retinal integrity at different ages, showing a correlation between integrity and age. In direct contrast, two other cross-sectional OCT studies show no correlation between retinal integrity and age and have suggested that the natural history is highly variable among subjects and that progressive cone loss is not inevitable in all subjects.[18,30] Interestingly, the subjects with *GNAT2*-associated ACHM and better cone structure were actually older than the subjects with *CNGA3/B3* mutations. Thus, if ACHM is generally progressive, our findings would indicate genotype-specific differences in the rate of progression.

With gene therapy trials planned in the near future, developing imaging protocols and analysis methods to both identify the best candidates for therapeutic intervention and assess the effect of intervention is essential. The cell reflectivity analyses presented here could be used for both aims. On the one hand, population-based measures of reflectivity could be used to evaluate differences in cone health among subjects: the thought being those with cones of greater reflectivity may have a greater therapeutic potential than those with cones of lesser reflectivity. An important question to be addressed is the role of numerosity in determining the therapeutic potential of a given subject: is it better to have fewer cones with better structure or more cones with worse structure (and perhaps variable response to treatment)? Cone reflectivity also may be useful in evaluating therapeutic efficacy after the initiation of treatment: in the case of successful restoration of cone structure and function, one might expect that the overall cone reflectance would increase. Direct tracking of individual photoreceptor reflectance over time, before and after treatment, may be a more sensitive metric to quantify early changes than visual function (Jonnal RS, et al. *IOVS* 2007;48:ARVO E-Abstract 1955).[33,36,46,47]

Acknowledgments

The authors thank Catey Bunce, UCL Institute of Ophthalmology, for statistical guidance. The authors would also like to thank Graham Holder and Anthony Robson, Moorfields Eye Hospital and UCL Institute of Ophthalmology, for their help and support in electrophysiological testing.

Supported by grants from the National Institute for Health Research Biomedical Research Centre at Moorfields Eye Hospital National Health Service Foundation Trust and UCL Institute of Ophthalmology; National Institutes of Health Grants R01EY017607, P30EY001931, and C06RR016511; Fight For Sight; Moorfields Eye Hospital Special Trustees; the Foundation Fighting Blindness; Retinitis Pigmentosa Fighting Blindness; and an unrestricted departmental grant (Medical College of Wisconsin) from Research to Prevent Blindness. Also supported by a multiuser equipment grant from The Wellcome Trust (099173/Z/12/Z); a Burroughs Wellcome Fund Career Award at the Scientific Interface and a Career Development Award from Research to Prevent Blindness (AD); and a Foundation Fighting Blindness Career Development Award (MM). Supported in part by the National Center for Advancing Translational Sciences, National Institutes of Health (Grant UL1TR000055). The authors alone are responsible for the content and the writing of the paper, and its contents do not necessarily represent the official views of the National Institutes of Health. Christopher Langlo is a member of the Medical Scientist Training Program at MCW, which is partially supported by a training grant from NIGMS T32-GM080202.

Disclosure: **A.M. Dubis**, None; **R.F. Cooper**, None; **J. Aboshiha**, None; **C.S. Langlo**, None; **V. Sundaram**, None; **B. Liu**, None; **F. Collison**, None; **G.A. Fishman**, None; **A.T. Moore**, None; **A.R. Webster**, None; **A. Dubra**, None; **J. Carroll**, None; **M. Michaelides**, None

References

1. Michaelides M, Hunt DM, Moore AT. The cone dysfunction syndromes. *Br J Ophthalmol*. 2004;88:291–297.
2. Andreasson S, Tornqvist K. Electroretinograms in patients with achromatopsia. *Acta Ophthalmologica*. 1991;69:711–716.
3. Sundin OH, Yang JM, Li Y, et al. Genetic basis of total colourblindness among the Pingelapese islanders. *Nat Genet*. 2000;3:289–293.
4. Wissinger B, Jägle H, Kohl S, et al. Human rod monochromacy: linkage analysis and mapping of a cone photoreceptor expressed candidate gene on chromosome 2q11. *Genomics*. 1998;51:325–331.
5. Kohl S, Baumann B, Rosenberg T, et al. Mutations in the cone photoreceptor G-protein alpha-subunit gene GNAT2 in patients with achromatopsia. *Am J Hum Genet*. 2002;71:422–425.
6. Chang B, Grau T, Dangel S, et al. A homologous genetic basis of the murine cpfl1 mutant and human achromatopsia linked to mutations in the PDE6C gene. *Proc Natl Acad Sci U S A*. 2009;106:19581–19586.
7. Kohl S, Coppieters F, Meire F, et al. A nonsense mutation in PDE6H causes autosomal-recessive incomplete achromatopsia. *Am J Hum Genet*. 2012;91:527–532.
8. Kohl S, Varsanyi B, Antunes GA, et al. CNGB3 mutations account for 50% of all cases with autosomal recessive achromatopsia. *Eur J Hum Genet*. 2005;13:302–308.
9. Galezowski X. *Du diagnostic des Maladies des Yeux par la Chromatoscopie rétinienne: Précéde d'une Etude sur les Lois physiques et physiologiques des Couleurs*. Paris: J.B. Baillière et Fils; 1868.
10. Larsen H. Demonstration mikroskopischer Präparate von einem monochromatischen Auge. *Klin Monbl Augenheilkd*. 1921;67:301–302.
11. Harrison R, Hoefnagel D, Hayward JN. Congenital total color blindness, a clinicopathological report. *Arch Ophthalmol*. 1960;64:685–692.
12. Falls HF, Wolter R, Alpern M. Typical total monochromasy—a histological and psychophysical study. *Arch Ophthalmol*. 1965;74:610–616.
13. Glickstein M, Heath GG. Receptors in the monochromat eye. *Vis Res*. 1975;15:633–636.
14. Dubra A, Sulai Y, Norris JL, et al. Non-invasive imaging of the human rod photoreceptor mosaic using a confocal adaptive optics scanning ophthalmoscope. *Biomed Opt Exp*. 2011;2:1864–1876.
15. Rossi EA, Chung M, Dubra A, Hunter JJ, Merigan WH, Williams DR. Imaging retinal mosaics in the living eye. *Eye (Lond)*. 2011;25:1–8.
16. Carroll J, Choi SS, Williams DR. In vivo imaging of the photoreceptor mosaic of a rod monochromat. *Vis Res*. 2008;48:2564–2568.

17. Merino D, Duncan JL, Tiruveedhula P, Roorda A. Observation of cone and rod photoreceptors in normal subjects and patients using a new generation adaptive optics scanning laser ophthalmoscope. *Biomed Opt Exp*. 2011;2:2189–2201.
18. Genead MA, Fishman GA, Rha J, et al. Photoreceptor structure and function in patients with congenital achromatopsia. *Invest Ophthalmol Vis Sci*. 2011;52:7298–7308.
19. Scoles D, Sulai YN, Langlo CS, et al. In vivo imaging of human cone photoreceptor inner segments. *Invest Ophthalmol Vis Sci*. 2014;55:4244–4251.
20. Xue B, Choi SS, Doble N, Werner JS. Photoreceptor counting and montaging of en-face retinal images from an adaptive optics fundus camera. *J Opt Soc Am A*. 2007;24:1364–1372.
21. Garrioch R, Langlo C, Dubis AM, Cooper RF, Dubra A, Carroll J. Repeatability of in vivo parafoveal cone density and spacing measurements. *Optom Vis Sci*. 2012;89:632–643.
22. Li KY, Roorda A. Automated identification of cone photoreceptors in adaptive optics retinal images. *J Opt Soc Am A*. 2007;24:1358–1363.
23. Chiu SJ, Lokhnygina Y, Dubis AM, et al. Automatic cone photoreceptor segmentation using graph theory and dynamic programming. *Biomed Opt Exp*. 2013;4:924–937.
24. Alexander JJ, Umino Y, Everhart D, et al. Restoration of cone vision in a mouse model of achromatopsia. *Nature Med*. 2007; 13:685–687.
25. Komáromy A, Alexander JJ, Rowlan JS, et al. Gene therapy rescues cone function in congenital achromatopsia. *Hum Mol Genet*. 2010;19:2581–2593.
26. Michalakis S, Muhlfriedel R, Tanimoto N, et al. Restoration of cone vision in the CNGA3-/- mouse model of congenital complete lack of cone photoreceptor function. *Mol Ther*. 2010;18:2057–2063.
27. Carvalho LS, Xu J, Pearson R, et al. Long-term and age-dependent restoration of visual function in a mouse model of CNGB3-associated achromatopsia following gene therapy. *Hum Mol Genet*. 2011;20:3161–3175.
28. Johnson S, Michaelides M, Aligianis IA, et al. Achromatopsia caused by novel mutations in both CNGA3 and CNGB3. *J Med Genet*. 2004;41:e20.
29. Tanna H, Dubis AM, Ayub N, et al. Retinal imaging using commercial broadband optical coherence tomography. *Br J Ophthalmol*. 2010;94:372–376.
30. Sundaram V, Wilde C, Aboshiha J, et al. Retinal structure and function in achromatopsia: implications for gene therapy. *Ophthalmology*. 2014;121:234–245.
31. Hood DC, Zhang X, Ramachandran R, et al. The inner segment/outer segment border seen on optical coherence tomography is less intense in patients with diminished cone function. *Invest Ophthalmol Vis Sci*. 2011;52:9703–9709.
32. Dubra A, Sulai Y. Reflective afocal broadband adaptive optics scanning ophthalmoscope. *Biomed Opt Exp*. 2011;2:1757–1768.
33. Cooper RF, Dubis AM, Pavaskar A, Rha J, Dubra A, Carroll J. Spatial and temporal variation of rod photoreceptor reflectance in the human retina. *Biomed Opt Exp*. 2011;2:2577–2589.
34. Dubra A, Harvey Z. Registration of 2D Images from fast scanning ophthalmic instruments. In: Fischer B, Dawant B, Lorenz C, eds. *Biomedical Image Registration*. Berlin: Springer; 2010;60–71.
35. Cideciyan AV, Hufnagel RB, Carroll J, et al. Human cone visual pigment deletions spare sufficient photoreceptors to warrant gene therapy. *Hum Gene Ther*. 2013;24:993–1006.
36. Jonnal RS, Besecker JR, Derby JC, et al. Imaging outer segment renewal in living human cone photoreceptors. *Opt Exp*. 2010; 18:5257–5270.
37. Abramoff MD, Magelhaes PJ, Ram SJ. Image processing with ImageJ. *Biophotonics International*. 2004;11:36–42.
38. Stockman A, Smithson HE, Michaelides M, Moore AT, Webster AR, Sharpe LT. Residual cone vision without alpha-transducin. *J Vis*. 2007;7(4):8,1–13.
39. Lazow MA, Hood DC, Ramachandran R, et al. Transition zones between healthy and diseased retina in choroideremia (CHM) and Stargardt disease (STGD) as compared to retinitis pigmentosa (RP). *Invest Ophthalmol Vis Sci*. 2011;52:9581–9590.
40. Carroll J, Neitz M, Hofer H, Neitz J, Williams DR. Functional photoreceptor loss revealed with adaptive optics: an alternate cause for color blindness. *Proc Natl Acad Sci U S A*. 2004;101: 8461–8466.
41. Carroll J, Dubra A, Gardner JC, et al. The effect of cone opsin mutations on retinal structure and the integrity of the photoreceptor mosaic. *Invest Ophthalmol Vis Sci*. 2012;53: 8006–8015.
42. Hansen SO, Cooper RF, Dubra A, Carroll J, Weinberg DV. Selective cone photoreceptor injury in acute macular neuroretinopathy. *Retina*. 2013;33:1650–1658.
43. Michaelides M, Aligianis IA, Ainsworth JR, et al. Progressive cone dystrophy associated with mutation in CNGB3. *Invest Ophthalmol Vis Sci*. 2004;45:1975–1982.
44. Thiadens AAHJ, Somervuo V, van den Born LI, et al. Progressive loss of cones in achromatopsia: an imaging study using spectral-domain optical coherence tomography. *Invest Ophthalmol Vis Sci*. 2010;51:5952–5957.
45. Thomas MG, Kumar A, Kohl S, Proudlock FA, Gottlob I. High-resolution in vivo imaging in achromatopsia. *Ophthalmology*. 2011;118:882–887.
46. Godara P, Cooper RF, Sergouniotis PI, et al. Assessing retinal structure in complete congenital stationary night blindness and Oguchi disease. *Am J Ophthalmol*. 2012;154:987–1001.
47. Pallikaris A, Williams DR, Hofer H. The reflectance of single cones in the living human eye. *Invest Ophthalmol Vis Sci*. 2003;44:4580–4592.

Investigative Ophthalmology & Visual Science